Hindawi
Advances in Civil Engineering
Volume 2022, Article ID 3979195, 24 pages
https://doi.org/10.1155/2022/3979195

Research Article

Performance Assessment of Reinforced Concrete Frame under Close-In Blast Loading

Solomon Abebe[1] **and Tesfaye Alemu Mohammed**[2]

[1]*Civil Engineering Department, Debre Markos University, Debre Markos, Ethiopia*
[2]*Civil Engineering Department, Addis Ababa Science and Technology University, Addis Ababa, Ethiopia*

Correspondence should be addressed to Tesfaye Alemu Mohammed; tes.alemu@gmail.com

Received 22 October 2021; Revised 25 January 2022; Accepted 9 March 2022; Published 27 March 2022

Academic Editor: Weifang Xiao

The need for assessing and retrofitting structures increased with time as terrorism-induced explosion trends rose with time. This paper presents a numerical investigation on performance assessment of a two-story, one-bay seismic resistant reinforced concrete framed building under close-in blast loading. ANSYS AUTODYN, an explicit nonlinear finite element software program, was used for 3D model development and analysis. The experimental results reported in the literature were used to validate proposed FE models. Furthermore, parametric studies on close-in explosive story-to-story locations and charge masses were performed on both conventional and seismically detailed RC framed structures. FEA results showed that a decrease in scaled distance raised effective plastic strain and damage index values. Furthermore, simultaneous use of close-spaced transverse steel reinforcement spacing in mid-height and ends of reinforced concrete columns is found to be effective in reducing both effective plastic strains and damage index values.

1. Introduction

Field blast explosion tests have been performed in a very controlled manner with the help of military supervision. In part, this testing arrangement high cost and associated risk of conducting field tests limited access for blast-related extreme loading studies. However, terrorism-related or accidental explosions have increased with time. Recently, the Beirut port explosion alone resulted in 15 billion USD in civil engineering infrastructure and property damages, with reported 7000 injuries and at least 220 deaths, according to Balsamos et al. [1].

Structures designed for conventional gravity and seismic loading are vulnerable to extensive damage when subjected to extreme blast loading. This is partly because conventional structures are designed and detailed for reduced seismic demands and have limited capacity to resist abnormally high impulsive extreme loads such as impact and blast loading [2, 3]. Previous studies focused on the investigation of individual reinforced structural members such as beams [4–6], columns [3, 7–9], and slabs [10–12] subjected to blast loading.

A few studies investigated the overall global response of reinforced concrete frames consisting of all slab, beam, and column structural members. Jayasooriya [2] performed vulnerability assessment and damage analysis of reinforced concrete-framed buildings subjected to near-field blast loading. The author implied the use of multisteel reinforcement cages and composite columns to resist blast loading. With the help of a commercially available software SAP2000, the authors in [13–15] conducted a numerical study on the behavior and response of multistory reinforced concrete buildings. Tewari and Sharma [16] studied the effect of blast load on the dynamic response of a high-story 3D RC frame by using STAAD Pro.

On the other hand, the authors in [17, 18] deployed ANSYS AUTODYN FE packaged software to evaluate the behavior and response of a plane frame structure under blast load. Williams et al. [17] determined the numerical response of a one-story, one-bay steel frame. The researchers modeled the steel plane frame by using a single degree of freedom, design to resist a given seismic load, and different blast load scenarios were deployed on the frame system by using a TNT

explosive. From the study results, the authors insisted that, during the blast loading event, the seismically designed plane frame was robust enough to enter plastic zones.

Moreover, Murali and Sujisha [18] studied the response of three-story, three-bay reinforced concrete bare frames, frames with and without brick infill walls, and brick infill walled frames with and without openings prone to blast loading. The frames were designed and detailed as ordinary moment-resisting frames, and then the 3D FEA modelling was employed by using the nonlinear computational program ANSYS AUTODYN. The authors generated the TNT explosive simulations from the AUTODYN module, and two blast-induced shock waves, namely, blast load with and without negative phase profiles, were considered. From the numerical study results, frames subjected to both positive and negative phases revealed maximum displacement values. In addition to this, infill walled frames with openings were found to be susceptible to large displacements.

On the other hand, Toy and Sevim [19] numerically investigated the structural response of a two-story, two-bay reinforced concrete building prone to blast load. The authors designed and detailed only one building model, especially an existing real building that bombed in August 2015 in Istanbul, and only one analysis was performed. Explicit analysis was employed by using the nonlinear FEA computational software ANSYS AUTODYN. Based on the FEA postprocessed results, the authors insisted on the complete collapse of nonstructural components. However, the structural elements of the frame suffered enormous damage including crushing of concrete and yielding of reinforcement bars.

Despite the efforts made by other researchers, it is obvious that the use of commercially available general FE software such as SAP2000 and STAAD Pro may not adequately represent different material models specifically generated for abnormal loads, such as blast load, and those software also hinder researchers and engineers to use and provide explicitly different reinforcement detailing schemes, which are in contrary easy on other research FEA software such as ANSYS AUTODYN. Consequently, some researchers have also made efforts by only considering the dynamic response of a plane frame system under blast loads. But this type of analysis method mismatches and does not capture the real dynamic behavior of spatial 3D models.

Thus, there is a void in the literature to study the global overall response of a reinforced concrete frame consisting of various interconnected structural members under extreme blast loading. Moreover, due to the complicated nature of explosions and the propagation of blast-induced shock waves, it is worthy to capture load transfer mechanisms among structural members and the global response of an RC frame under blast loading by 3D modelling and analyzing of the RC frame. Also, the boundary conditions deployed for individual RC slabs, beams, and columns are all simplified and prescribed support conditions. However, 3D modelling of frames consisting of individual structural members as an interconnected framework offers options to evaluate structural joint performance in FE analysis. Currently, advances in finite element analysis and the availability of high-speed computing have enabled spatial 3D model development of reinforced concrete frames subjected to blast loading simulation analysis.

Therefore, this study fills a perceived void in the literature by studying the structural response of two-story, one-bay, reinforced concrete frames with and without seismic detail provisions, under extreme close-in blast loading. Variable axial loads induced by dynamic reactions of beams and slabs caused by the effects of indoor explosions on supported masses are all captured. Field test data reported in literature [20] were used for validation finite element analysis, and further parametric studies on story-to-story close-in explosive locations, charge masses, and various reinforcement detailing schemes were performed on both conventional and seismically detailed RC framed structures.

2. Description of Numerical Model

ANSYS AUTODYN [21] software program was used for 3D model development, blast loading, and finite element simulation analysis. Next, details of employed material models, boundary conditions, blast loading application, and FE procedures are presented.

2.1. Material Models. The RHT material model which was originally developed by Riedel–Heirmaier–Thoma was implemented in the nonlinear computational program ANSYS AUTODYN [21] and is extensively used in finite element analysis of reinforced concrete structures under blast loading. Experimental and field blast tests were used by various authors to verify and validate their accuracy [22–25]. The authors insisted that the RHT material model united strain rate effect, equation of state (EOS), plasticity, and three failure surface caps, namely, inelastic yield, postfailure, and residual surface features to simulate concrete dynamic strength behavior for extreme loading, such as impact and blast loads. The model uses about 30 input parameters including hydrostatic compression, uniaxial tension, and uniaxial and triaxial compression parameters.

EOS describes the hydrodynamic response of a concrete material when subjected to accidental loads such as blast loading, which is assumed as hydrodynamic, with pressure varying as a function of density and internal energy [25].

In the present study, the RHT concrete material model was used to characterize concrete. Input parameters for the RHT concrete material model are presented in Tables 1–4 in terms of P-alpha, polynomial equation of states, concrete strength, and damage (failure) values.

According to [22–25], material damage is initiated, if further plastic damage occurs after the initial failure surface is reached. The model evaluates damage parameter D using equation (1). The logic behind the damage formulae is the accumulation of increments of effective plastic strain.

$$0 \le D = \sum \frac{\Delta \varepsilon_{pl}}{\varepsilon_f (p)} \le 1, \tag{1}$$

where $\varepsilon_f (p)$ is the failure strain and can be calculated as listed in

Table 1: P-alpha EOS input parameters for C-35 concrete.

Variable	Meaning	Value/remark
$\rho_{\text{solid},o}$	Reference density (kg/m^3)	2750
ρ_{porous}	Porous density (kg/m^3)	2314
c_e	Porous sound-speed (m/s)	$2.92E+3$
p_{el}	Initial compaction pressure (kPa)	$2.33E+4$
p_S	Solid compaction pressure (kPa)	$6.00E+6$
n	Compaction exponent	3.0
T_{ref}	Reference temperature (°C)	26.85

Table 2: Polynomial EOS input parameters for C-35 concrete.

Variable	Meaning	Value/remark
A_1	Bulk modulus matrix (kPa)	$3.53E+7$
A_2	Parameter A_2 (kPa)	$3.96E+7$
A_3	Parameter A_3 (kPa)	$9.04E+6$
B_0	Parameter B_0	1.22
B_1	Parameter B_1	1.22
T_1	Parameter T_1 (kPa)	$3.53E+7$
T_2	Parameter T_2 (kPa)	0.00

Table 3: RHT concrete strength model parameters for C-35 concrete.

Variable	Meaning	Value/remark
G	Shear modulus (GPa)	16.7
f_c	Compressive strength (MPa)	35.0
CAP	Use CAP on elastic surface?	Yes
f_t/f_c	Tensile strength	0.10
f_s/f_c	Shear strength	0.18
A_{fail}	Intact failure surface constant	1.60
n_{fail}	Intact failure surface constant	0.60
$Q_{2.0}$	Tension/compression meridian ratio	0.6805
BQ	Brittle to ductile transition	0.0105
S	Hardening slope	2.00
Tensrat	Elastic strength/f_t	0.7
Comprat	Elastic strength/f_c	0.53
B_{frac}	Fracture strength constant	1.6
n_{frac}	Fracture strength exponent	0.61
α	Compressive strain rate exponent	0.032
δ	Tensile strain rate exponent	0.036

Table 4: RHT failure model input parameters for C-35 concrete.

Variable	Meaning	Value/remark
SFMAX	Maximum fracture strength ratio	$1E+20$
D_1	Damage constant	0.04
D_2	Damage constant	1.00
$\varepsilon_{f,\text{min}}$	Minimum strain failure	0.01
G_{res}	Residual shear modulus fraction	0.13
EROSION	Use EROSION	Yes

$$\varepsilon_f(p) = D_1\left(p^f - p_t^*\right)^{D_2} \geq \varepsilon_{\min}, \tag{2}$$

where D_1, D_2, p_t^*, and $\varepsilon_{f\,\min}$ are input parameters [22–25] and also see Table 4 for RHT material model failure input parameters.

Activating the EROSION option enables the computational engine of AUTODYN to cross check strain limits of elements and eliminate an element in a finite element model if predefined strain limits were exceeded.

Ekstrom [26] investigated concrete structure dynamic response damage and fracture energy characteristics due to blast-induced shock waves. The author showed tensile fracture energy influenced the accuracy of FEA results than strain rate material properties. Table 5 presents input parameters for the Johnson–Cook strength model, which was used for steel rebar material characterization. Similarly, Table 6 exhibits the JWL input parameters for equivalent

TNT explosives. The JWL EOS input parameters were validated using different field test cases, computational programs, and explosion field events using entropy-based thermodynamic equations [27–30].

Blast-induced shock waves cannot propagate through vacuum. Atmospheric air was modeled to characterize blast-induced shock wave propagation through the air medium. Table 7 presents the required parameter inputs for modelling atmospheric air parameters in current numerical models.

Tables 1–7 detail input parameters listing and also provide an illustrative example for fellow researchers using RHT, Johnson–Cook, and JWL material models to characterize concrete, steel rebar, ANFO, and TNT explosive materials, and air for atmospheric pressure, respectively.

2.2. Element Types. A Lagrangian solid element was used to model the concrete column and substructure. Substructure or base material was modeled for purpose of reflecting blast-induced shock waves. The strength along the compressive meridian is expressed as a triaxial compression normalized to the unconfined compression strength f_c in the AUTODYN solver in the following equation by Brannon and Leelavanichkul [22]:

$$Y^*_{TXC} = \frac{Y_{TXC}}{f_c} = a_1\left[\frac{p}{f_c} - \frac{p_{\text{spall}}}{f_c} r_f\right]^{a_2}, \quad (3)$$

where $r_f = \begin{cases} (\varepsilon'/\varepsilon'_o)^{\alpha}: \ p > f_c \text{ with } \varepsilon'_o = 30x10^{-6}s{-}1 \\ (\varepsilon'/\varepsilon'_o)^{\beta}: \ p < f_c \text{ with } \varepsilon'_o = 3x10^{-6}s{-}1 \end{cases}$.

a_1 = initial slope of failure surface, a_2 = pressure dependency of failure surface, p_{spall} = spall strength, and α and β = material constants.

The solid element supports material and geometric nonlinearity and has 8 nodes with three displacement, velocity, and acceleration DOFs per node in X, Y, and Z directions. Steel reinforcements are modeled using a two—node element resisting only tensile and compressive forces. The element is compatible with concrete solid element and has three displacement, velocity, and acceleration DOFs per node in X, Y, and Z directions.

2.3. Modelling of TNT Explosive. Pressure-volume-energy behavior of TNT explosion with different charge masses in ANSYS AUTODYN input parameters can be determined using equation (4) of Jones–Wilkins–Lee (JWL) EOS [27, 30].

$$P = A\left(1 - \frac{\omega}{R_1 V}\right)e^{-R_1 V} + B\left(1 - \frac{\omega}{R_1 V}\right)e^{-R_2 V} + \frac{\omega E}{V}, \quad (4)$$

where P is pressure and v is volume relative to undetonated state (v/v_o). The parameters A, B, R_1, and R_2 are constants, and parameter ω is an assumed-constant material property.

While having 1 m height and different a diameter of a cylindrical TNT explosive container, the volume of the container is mapped after specifying the diameter of the cylindrical container. In other words, different charge masses of TNT are deployed by fixing the height and varying the diameter values. After establishing the required volume of TNT explosive, the locations for detonation points are defined by specifying X, Y, and Z coordinates.

2.4. Boundary and Loading Conditions. Column bottom translation and rotational degrees of freedom are constrained. Similarly, a concrete-based substructure is also restrained from translation and rotation on each side and bottom faces. The gravitational acceleration of 9.81 m/s^2 is applied to account for self-weight of the frame elements.

2.5. Nonlinear Finite Element Analysis Computation. ANSYS AUTODYN [21] nonlinear finite element software program is used to analyze and simulate reinforced concrete frames subjected to blast loading. Automatic explicit time steps and damping controls of 0.2 and 1 value are used for linear and quadratic artificial viscosity. An AUTODYN standard is also employed to control the hourglass damping.

3. Numerical Model Validation

3.1. Description of Validated Field Test (Specimen CONV_20). The field test results reported by Siba [20] are used for validation finite element analysis. The specimen designated as CONV_20 has 300 mm × 300 mm cross-sectional dimensions, 3200 mm height, and 41 MPa concrete compressive strength. The column is reinforced with 4–25 M and has 300 mm tie spacing (Figures 1 and 2).

Siba [20] performed the blast test at 2.6 m standoff distance with 150 kg ANFO explosive material yielding a 052 m/kg$^{1/3}$ scaled distance. The experimental test column displacement values were traced by deploying displacement gauge control points. Figure 3(a) shows the field test set up of the CONV_20 RC column, whereas Figure 3(b) exhibits its corresponding FE developed model using the ANSYS AUTODYN [21] software program.

3.2. Mesh Technique and Convergence. The mesh techniques were used for the simulation of solid materials, and a well-known so-called Lagrangian mesh technique with less computational cost was used. The mesh in the Lagrange tracks the material as it deforms, and the material stays inside the original element grid. In order to control the solution accuracy, especially in case of highly distorted meshes, controlling mechanisms including hourglass control, rezoning, and remapping options were activated in the ANSYS AUTODYN computational program.

Consequently, the mesh sensitivity study is a critical step to optimize computational demands and the accuracy of finite element results. In this research, preliminary analyses were performed using different mesh sizes of 20 mm, 25 mm, 30 mm, and 40 mm (see also Figure 4) and for final analysis, a fine mesh of 20 mm with same aspect ratio is selected for all subsequent FEA.

Nodal displacement values are traced by employing a displacement control point (gauge) located at lower one-third of the column (1 m). Figure 5 exhibits the nodal displacement values for different mesh sizes (see also Table 8).

Table 5: Johnson–Cook strength model input parameters for S400 rebar.

Variable	Meaning	Value/remark
ρ_{ref}	Reference density (kg/m^3)	7850
E	Young's modulus (GPa)	200
ν	Poisson's ratio	0.3
K	Bulk modulus (GPa)	166
C_ν	Specific heat (J/kgC)	434
SRCR	Strain rate correction	1st order
f_y	Initial yield stress (MPa)	400
HC	Hardening constant	510
f_y	Principal tensile failure stress (MPa)	600
STCN	Strain rate constant (MPa)	0.01
TSE	Thermal softening exponent (MPa)	1.03
MT	Melting temperature (°C)	1793
RSTR	Reference strain rate (sec^{-1})	1.00
Erosion	Erosion strain (%)	None
EOS	Equation of state	Linear

Table 6: JWL model input parameters for TNT explosive.

Variable	Meaning	Value/remark
ρ	Density (kg/m^3)	1630
A	Parameter A (GPa)	374
B	Parameter B (MPa)	375
R_1	Parameter R_1	4.15
R_2	Parameter R_2	0.90
W	Parameter W	0.35
C–J DV	C–J detonation velocity (m/s)	6930
C–J E	C–J energy/unit mass (J/kg)	$3.68E+6$
C–J P	C–J pressure (GPa)	0.2

Table 7: Atmosphere air input parameters for air medium.

Variable	Meaning	Value/remark
ρ	Density (kg/m^3)	1.225
C_ν	Specific heat (J/kgC)	717.6
Υ	Adiabatic exponent	1.40
T_{ref}	Reference temperature (°C)	26.85

3.3. Field Test and Numerical Model Comparison. Figures 6(a) and 6(b) present the blast wave propagation of field tests and FEA simulations during the blasting event. After the detonation of the ANFO explosive, which was contained in a cylindrical shape, the fireball engulfed the reinforced concrete column. The video recording during the experimental test carried out by Siba [20] did not show the response of the column; however, the evolution of the blast pressure and fireball was captured and a similar blast wave simulation was made by AUTODYN.

During the experimental test, Siba [20] embedded a string potentiometer at the front face of a column, and a displacement value of 11.2 mm was measured from the lower one-third region of the study column. Figure 7 elucidates a comparison of displacement-time history plots for experimentally reported data (CONV_20 RC column) and an FEA model with different mesh sizes extracted from a 1 m displacement control (gauge) point.

Moreover, posttest results for CONV_20 revealed that an extensive cracking and spalling of concrete in the lower one-third region of the column was obtained. After activating concrete EROSION option for the damage simulation, from the postprocessed results of damage scalar values, FEA model experienced the same extent of concrete crushing at the same location, i.e. the lower part of the column (see Figure 8).

Thus, FE validation analysis results including displacement threshold values and postblast damages from ANSYS AUTODYN are in good agreement with field test data reported by Siba [20]. This affirms use of the RHT concrete constitutive model, Johnson–Cook material model for reinforcement bars, and the JWL model for simulating explosions yields acceptable values for simulation of RC structural members under blast loading. Next, a detailed finite element simulation of a full-scale two-story one-bay reinforced concrete framed structure is presented.

4. Finite Element Simulation

4.1. RC Frame Models Reinforcement Detailing. In this section, responses of two-story, one-bay reinforced concrete

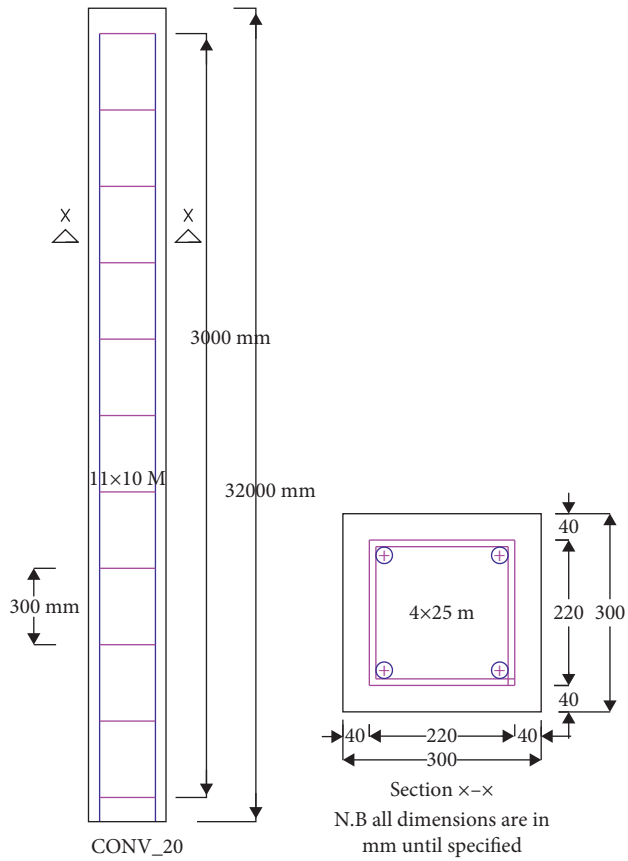

Figure 1: Sketch for CONV_20 RC column.

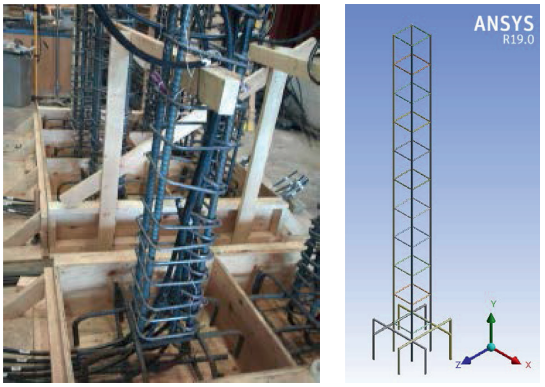

Figure 2: Reinforcement bar arrangement for CONV_20 RC column: (a) experiment carried out by Siba [20]; (b) AUTODYN FEA simulation.

frames, conventional (seismic deficient), and seismically detailed schemes subjected to various close-in blast loading are presented. Figures 9–15 present reinforcement details of conventional seismic deficient and seismically detailed RC columns. Conventional and seismic resistant RC columns are detailed as per EN 1992-1 EuroCode2 [31] and EN 1998-1:2003 EuroCode8 [32], respectively. All columns and beams had 300 mm × 300 mm cross-sections reinforced with 8ϕ12 mm and 6ϕ12 mm longitudinal bars, respectively. The spacing of transverse bars with ϕ8 mm ties is detailed to have different spacing along with the height of beam and column. FRM_REI_DET_#1 represents conventional frame for only gravity loading only, whereas FRM_REI_DET_#2 and FRM_REI_DET_#3 are seismic resistant frames.

5. Parametric Study Results and Discussions

In this section, a numerical study using the nonlinear computational FEA program, ANSYS AUTODYN, on effect of different reinforcement detailing provisions on a two-story one-bay RC framed structure under a blast-induced shock wave is presented. Figure 16 elucidates the indoor

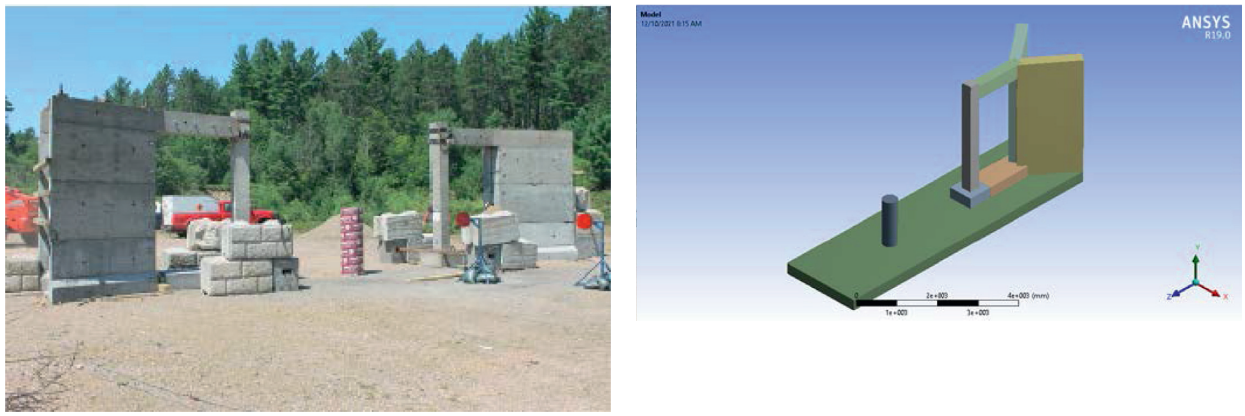

(a) (b)

Figure 3: CONV_20 test column and location of 150 kg ANFO explosive: (a) experiment carried out by Siba [20]; (b) AUTODYN FEA simulation.

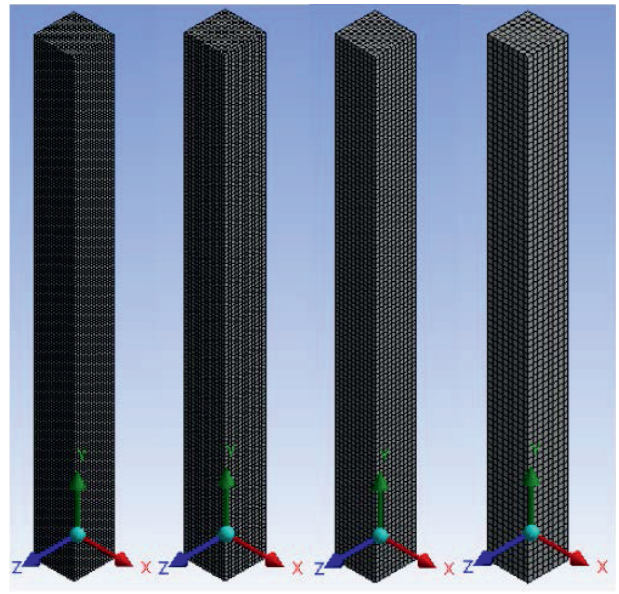

(a) (b) (c) (d)

Figure 4: AUTODYN FEA model for CONV_20 RC column with different mesh sizes: (a) 20 mm; (b) 25 mm; (c) 30 mm; (d) 40 mm.

location of equivalent TNT explosives, simulating various blast loading scenarios used in the present parametric study.

The parametric study consisted of three blast scenarios with reference to two blast points specifically located at the middle of the 1st and 2nd story levels. The first blast scenario had 46 kg TNT explosive charge mass and a 0.50 m/kg$^{1/3}$ scaled distance, whereas in the second blast load case, a 91 kg TNT explosive charge mass was applied yielding a 0.40 m/kg$^{1/3}$ scaled distance. The third blast scenario had a 215 kg TNT explosive charge mass with 0.30 m/kg$^{1/3}$ scaled distance.

The 3D frame had a 5 m × 5 m planar area and a 3 m floor height. In addition to the self-weight of each structural member (column, beam, and slab), 10 kN/m^2 live load characterized by the functional use of the floor system is imposed on 1st and 2nd story floor slabs.

Among the structural elements of a building, the column is a critical structural element subjected mainly to compression with/without bending, and is highly susceptible to early failure due to blast loading. Consequently, damage on columns trigger a whole frame system into progressive collapse. Thus, average damage index and effective plastic strain values were extracted from AUTODYN's postprocessed data files for the first and second story columns. Figure 17 elucidates ANUTODYN FEA models with indoor locations of TNT explosive, 3D model with and without meshes.

Sample detonation phases of TNT explosive on the 1st and 2nd floors with respective pressure values on the 3D FEA model are presented in Figure 18. Blast modelling is made by using ANSYS AUTODYN software and explicit analysis of those frames with and without seismic detailing provisions is performed for close-in extreme blast load cases. For a TNT explosive charge mass located on the first floor, ground floor columns suffered greater pressure than 2nd floor columns and on the contrary,

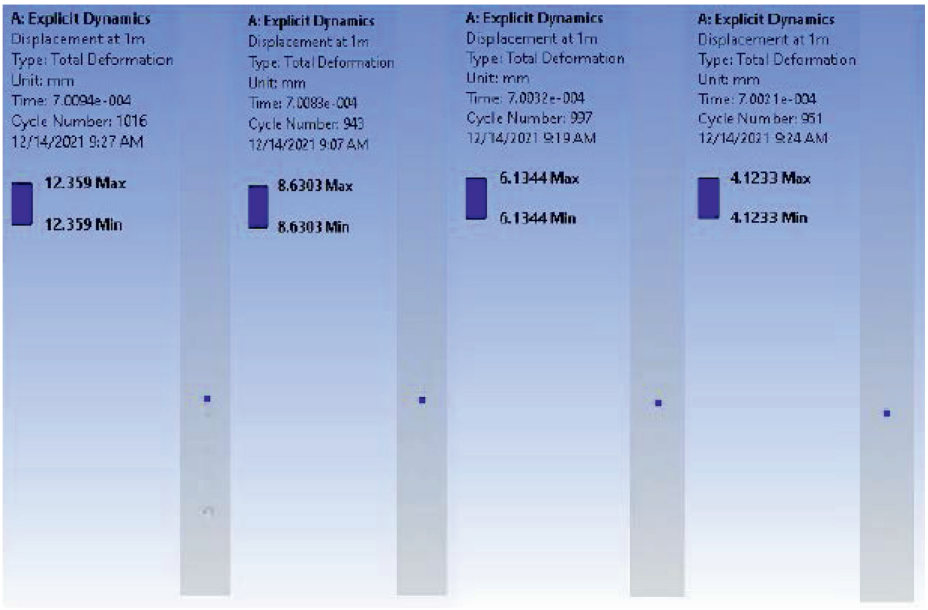

(a) (b) (c) (d)

Figure 5: Nodal displacement value for CONV_20 RC column located at 1 m control point: (a) 20 mm; (b) 25 mm; (c) 30 mm; (d) 40 mm.

Table 8: Mesh sensitivity analysis.

Mesh size (mm)	No. of nodes	No. of elements	Time elapsed (s)	Maximum displacement at lower one-third (mm)
20	43779	38250	1500	12.35
25	23153	19584	1080	8.63
30	13915	11400	960	6.14
40	6966	5440	900	4.12

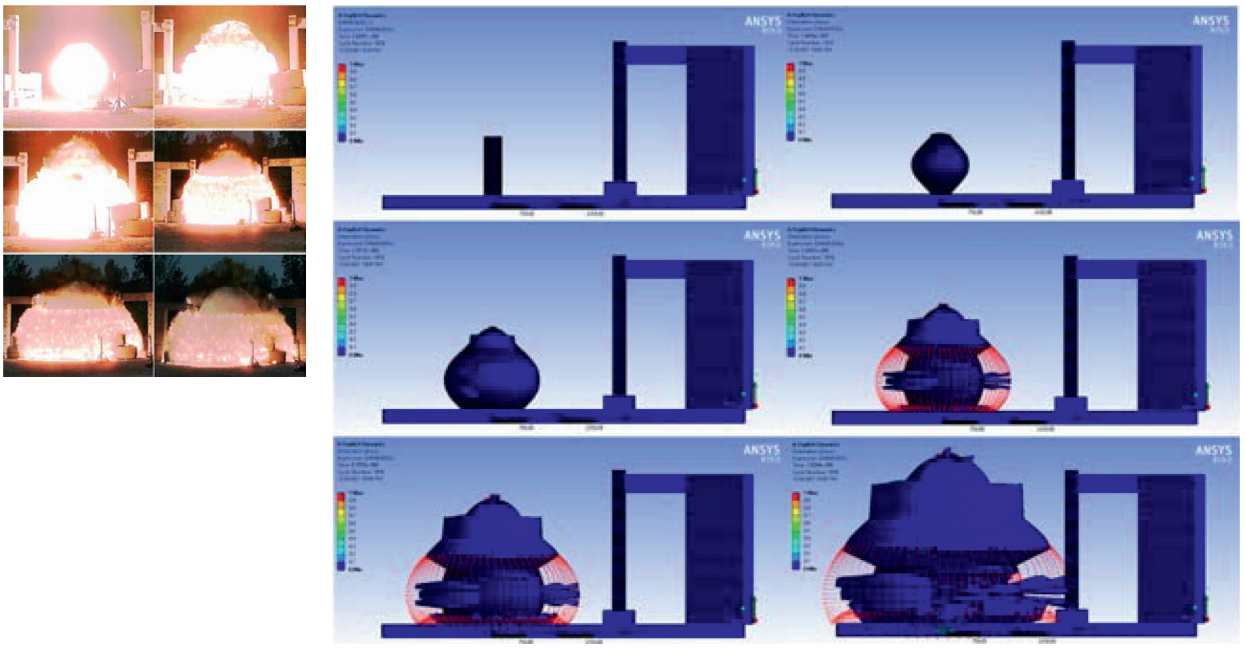

(a) (b)

Figure 6: Blast wave propagation: (a) field test carried out by Siba [20]; (b) FEA simulation.

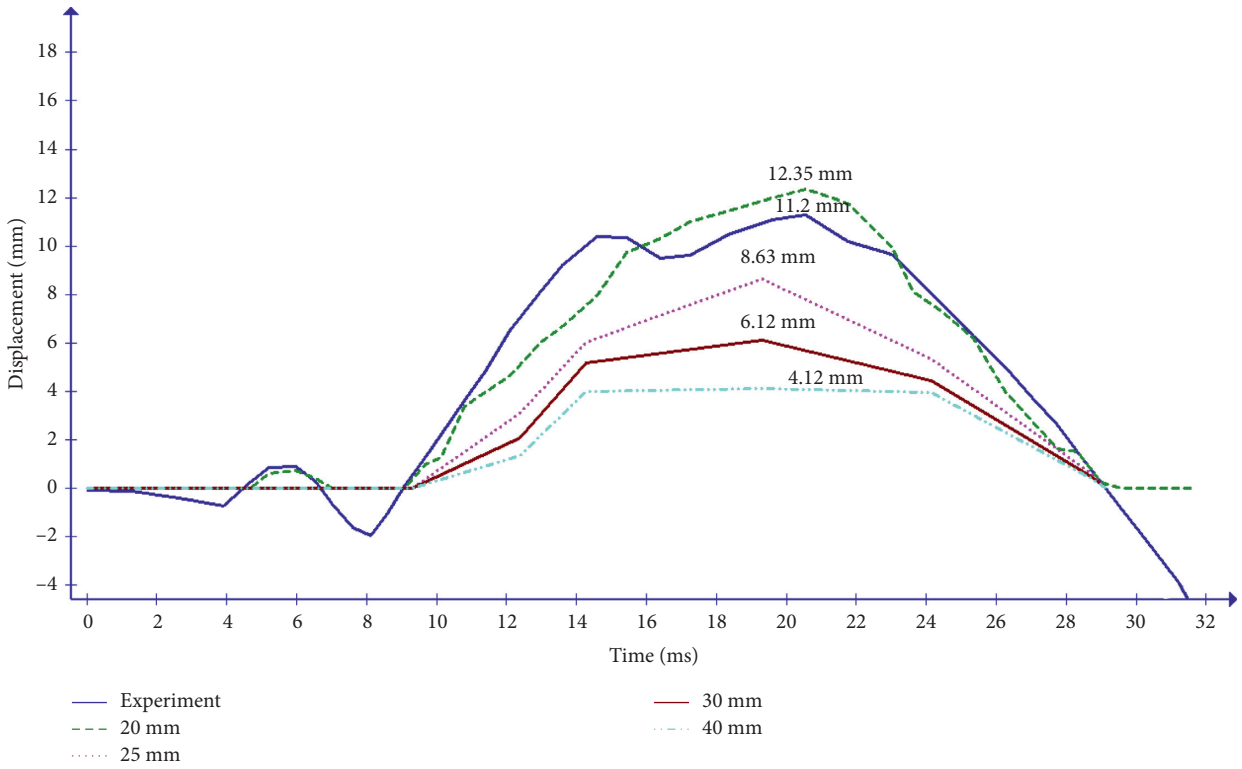

Figure 7: Displacement-time history curves for CONV_20 RC column with different mesh sizes.

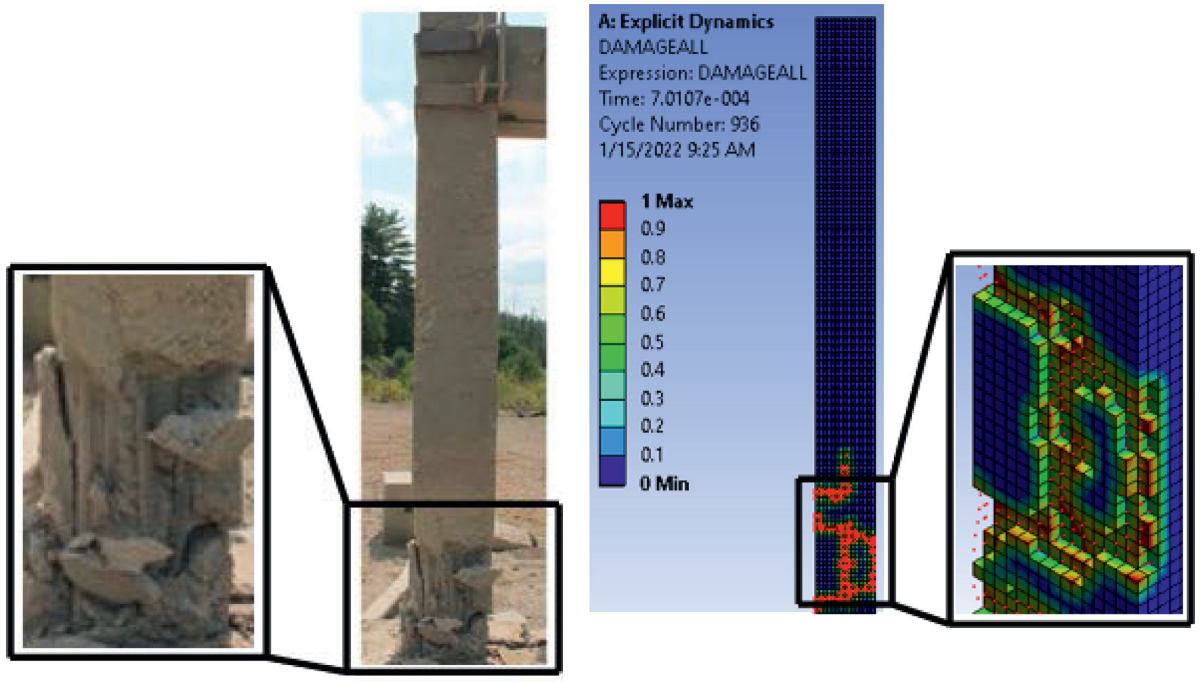

(a) (b)

Figure 8: Posttest photograph of column: (a) field test carried out by Siba [20] and (b) FE validation result.

when the TNT explosive is allowed to detonate in the 2nd floor, columns located on the respective floor are exposed to maximum blast-induced shock waves (Figure 18).

5.1. Blast Loading Response of Seismically Detailed Two-Story One-Bay RC Building Frame. This section presents a performance assessment of the seismically detailed RC frame

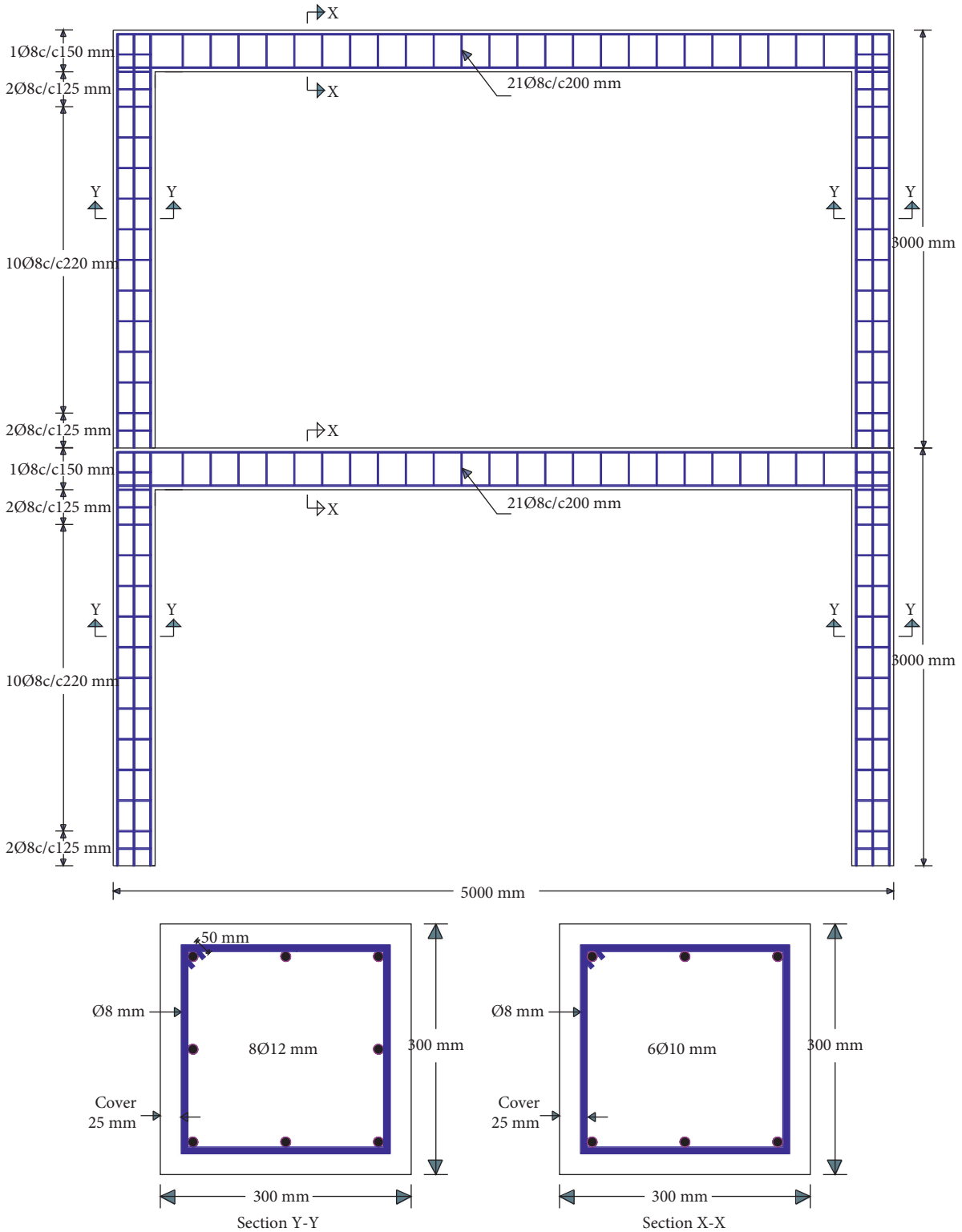

Figure 9: Reinforcement detailing for FRM_REI_DET_#1.

under blast loading. One conventional RC frame, FRM_REI_DET_#1, and two seismically detailed RC frames, FRM_REI_DET_#2 and FRM_REI_DET_#3, are studied with two probable indoor explosion locations (1st and 2nd story floor levels) and three different equivalent TNT explosive material charge masses (46 kg, 91 kg, and 215 kg).

FE numerical analysis results showed as charge mass increases, damage and effective plastic strain values also

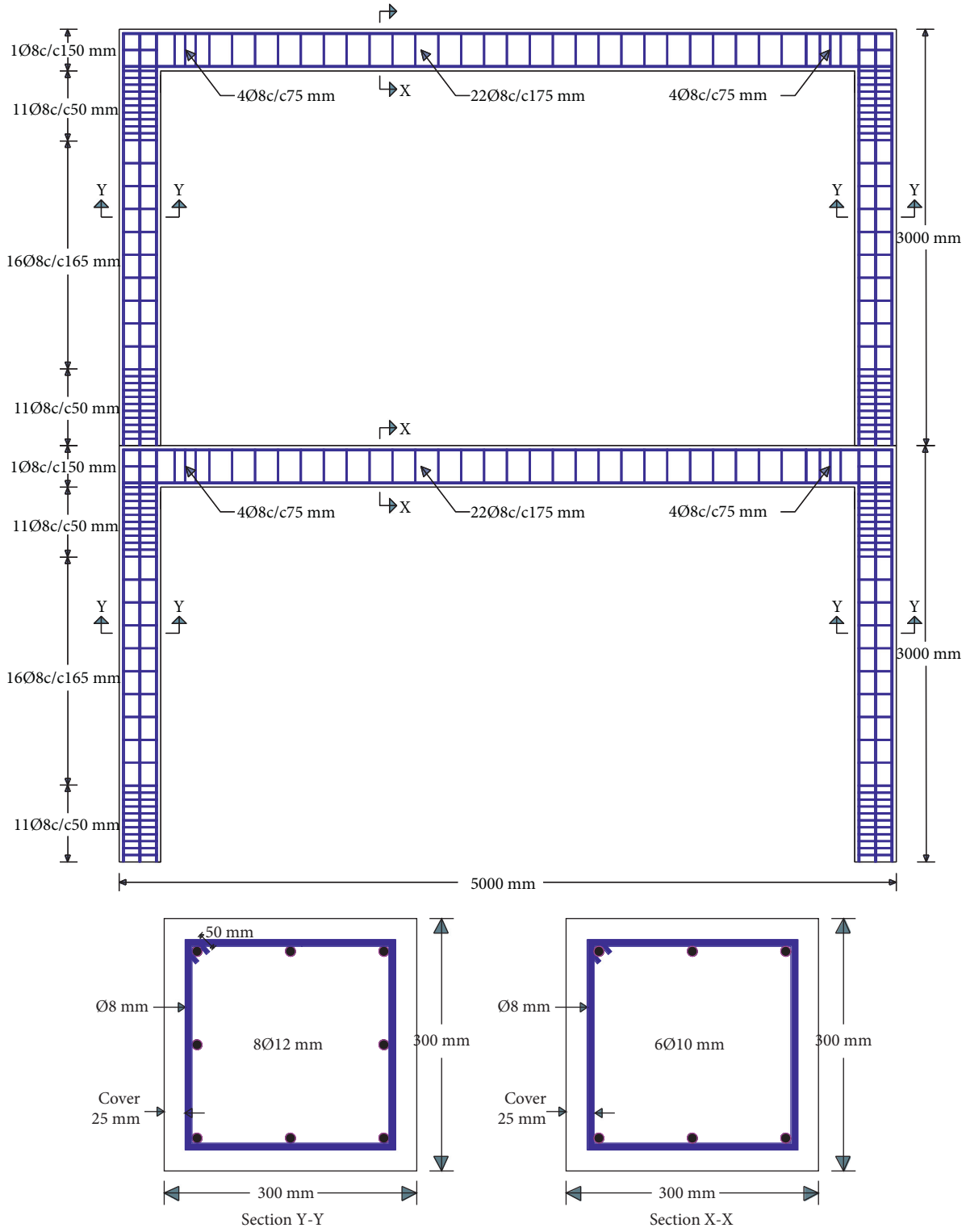

Figure 10: Reinforcement detailing for FRM_REI_DET_#2.

peaked. Moreover, as compared to conventionally detailed RC frames (FRM_REI_DET_#1), seismically detailed RC frames (FRM_REI_DET_#2 and FRM_REI_DET_#3) performed well under blast loading. For 0.50 m/kg$^{1/3}$ scaled distance, where TNT explosive is kept at 1st floor, and damages are reduced by 14.3% and 62% for RC frames FRM_REI_DET_#2 and FRM_REI_DET_#3, respectively (Figure 19). On the other hand, when TNT explosive is placed at 2nd story, the values are 16.7% and 62.5% (see Figure 20).

Similarly, for a 0.40 m/kg$^{1/3}$ scaled distance where TNT explosive is located at the 1st story floor level, 11.8% and 47.1% drop in damage values are observed (Figure 21). On the other

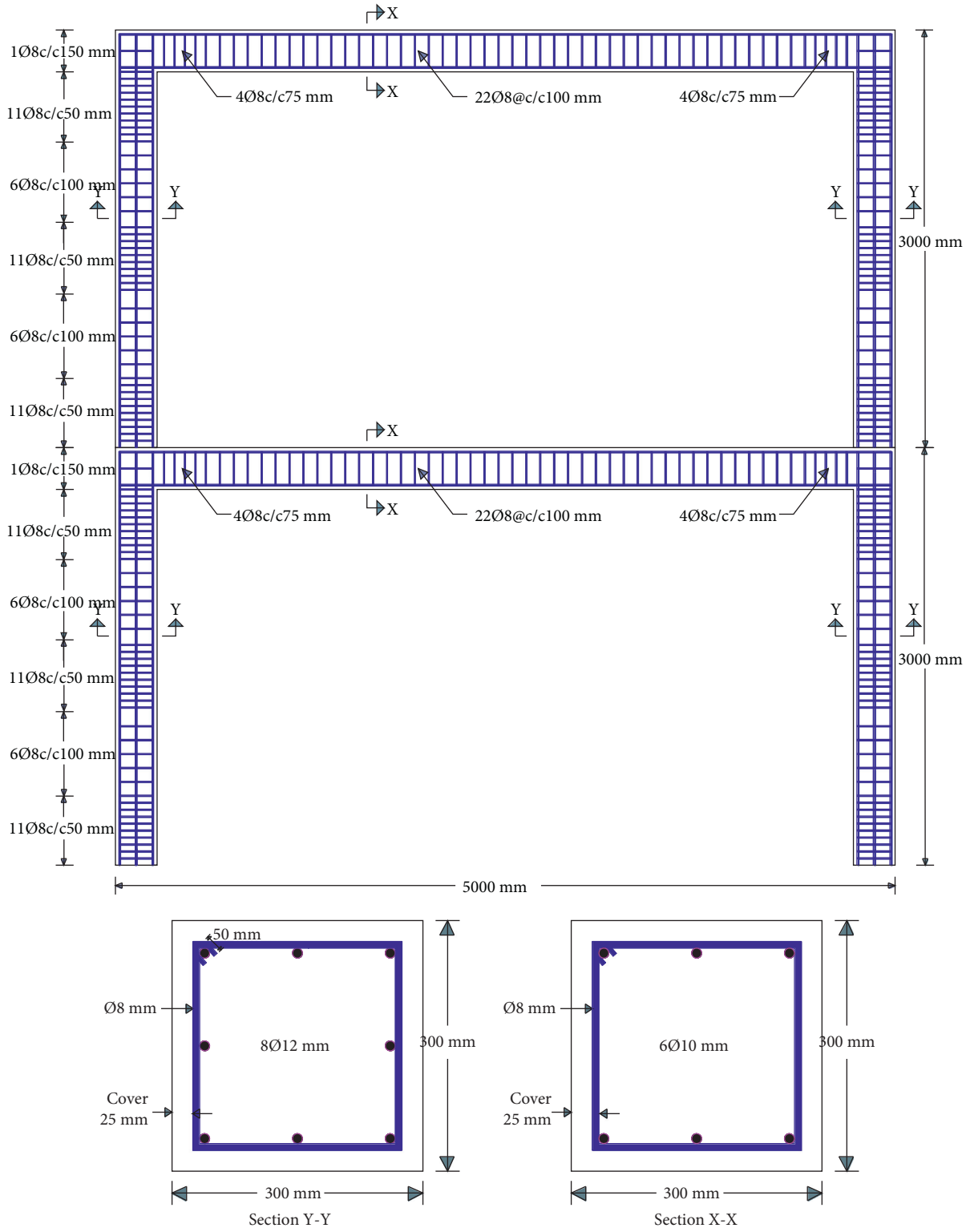

Figure 11: Reinforcement detailing for FRM_REI_DET_#3.

hand, for TNT explosive with the same 0.40 m/kg$^{1/3}$ scaled distance kept at 2nd story, decrease in damage value up to 10% and 47.5%, respectively, was observed (see Figure 22).

Figures 23 and 24 show performance gain of applying explosives with 0.30 m/kg$^{1/3}$ scaled distance at 1st and 2nd story floor levels, and damages lessened by 10%, 56.4% and 9.5%, 56.4%, respectively were recorded for FRM_REI_-DET_#2 and FRM_REI_DET_#3 RC frames, respectively.

Figures 25 and 26 present a summary of the performance of seismic deficient and seismically detailed columns. From the

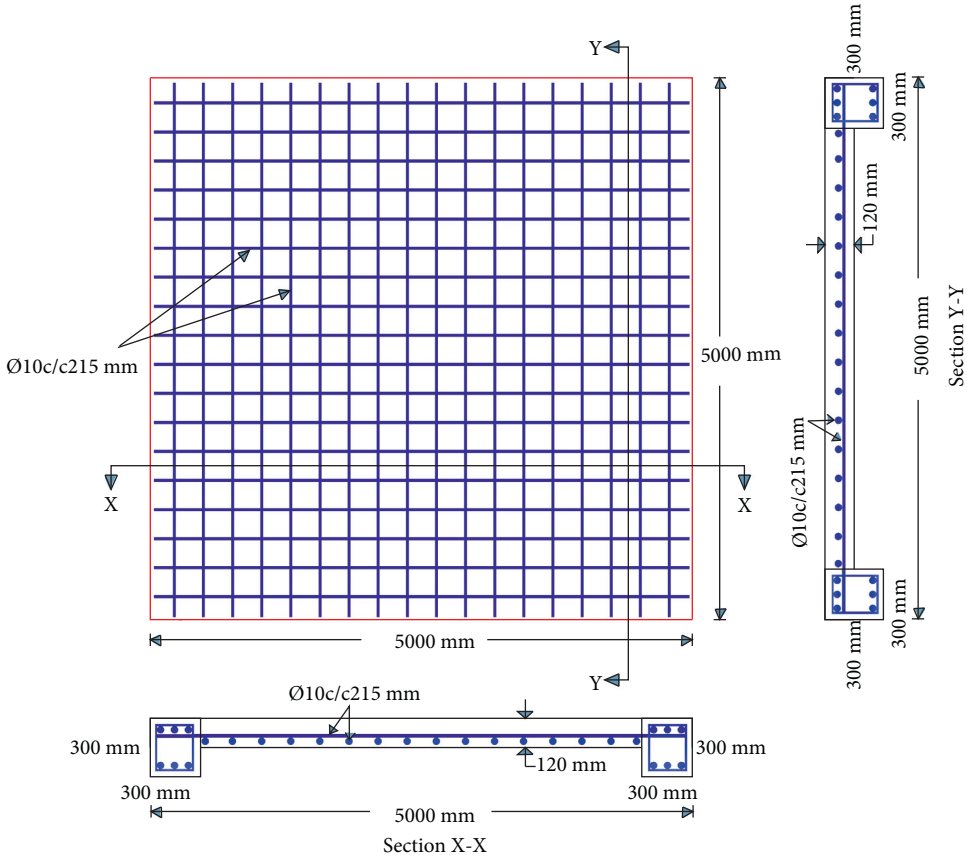

(a)

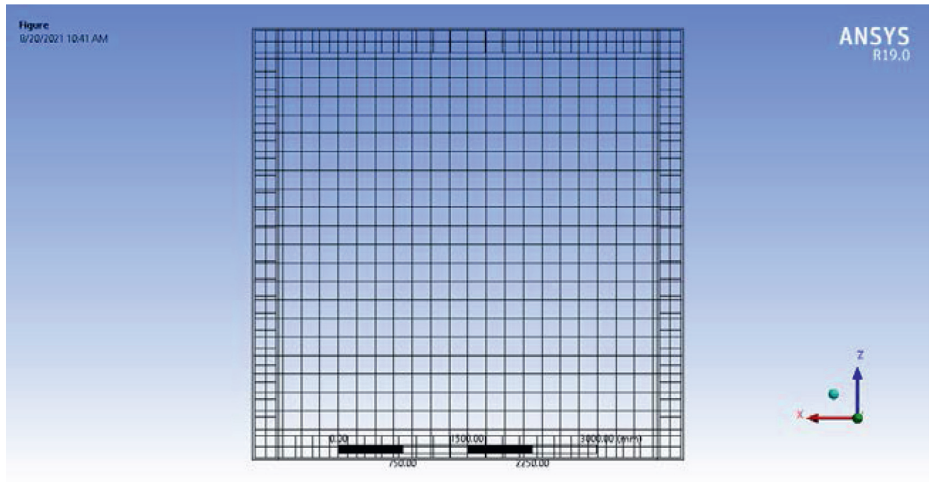

(b)

Figure 12: Solid slab reinforcement detailing for FRM_REI_DET_#1, FRM_REI_DET_#2, and FRM_REI_DET_#3 models: (a) sketch; (b) FEA model.

plot, it is evident that a decrease in scaled distances from 0.50 m/kg$^{1/3}$ to 0.30 m/kg$^{1/3}$ induced severe damages to the columns especially FRM_REI_DET_#1 and FRM_REI_DET_#2. On the contrary, FRM_REI_DET_#3 showed an incredible performance and robust resistance against close-in explosion scenarios.

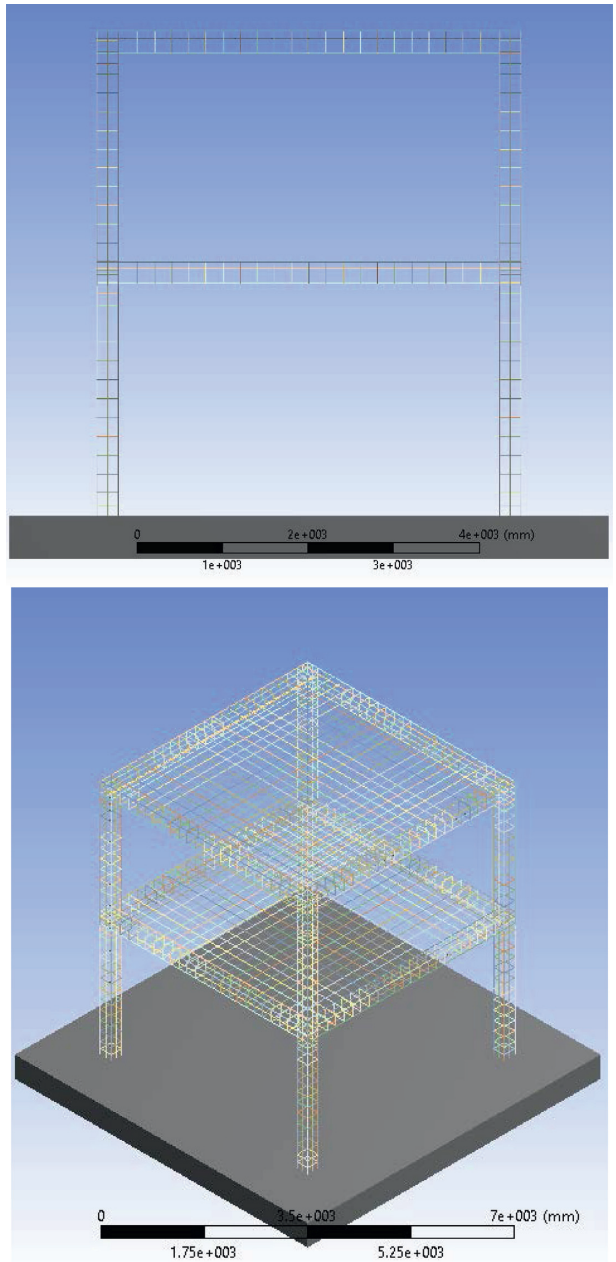

Figure 13: Reinforcement detailing for FRM_REI_DET_#1 on AUTODYN.

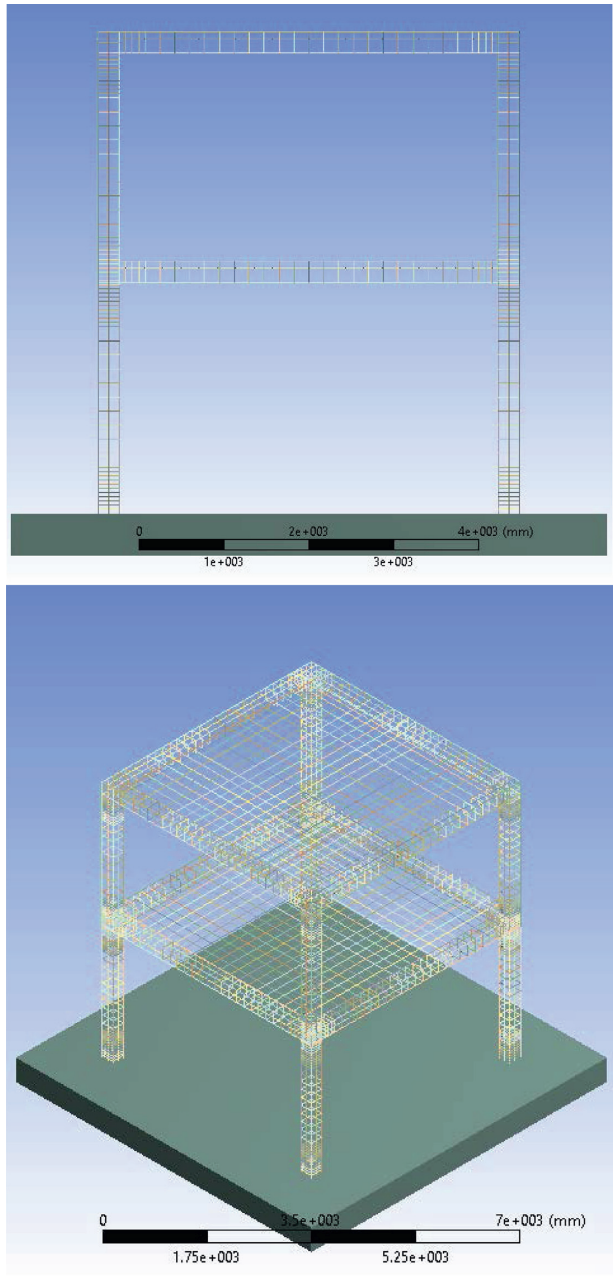

Figure 14: Reinforcement detailing for FRM_REI_DET_#2 on AUTODYN.

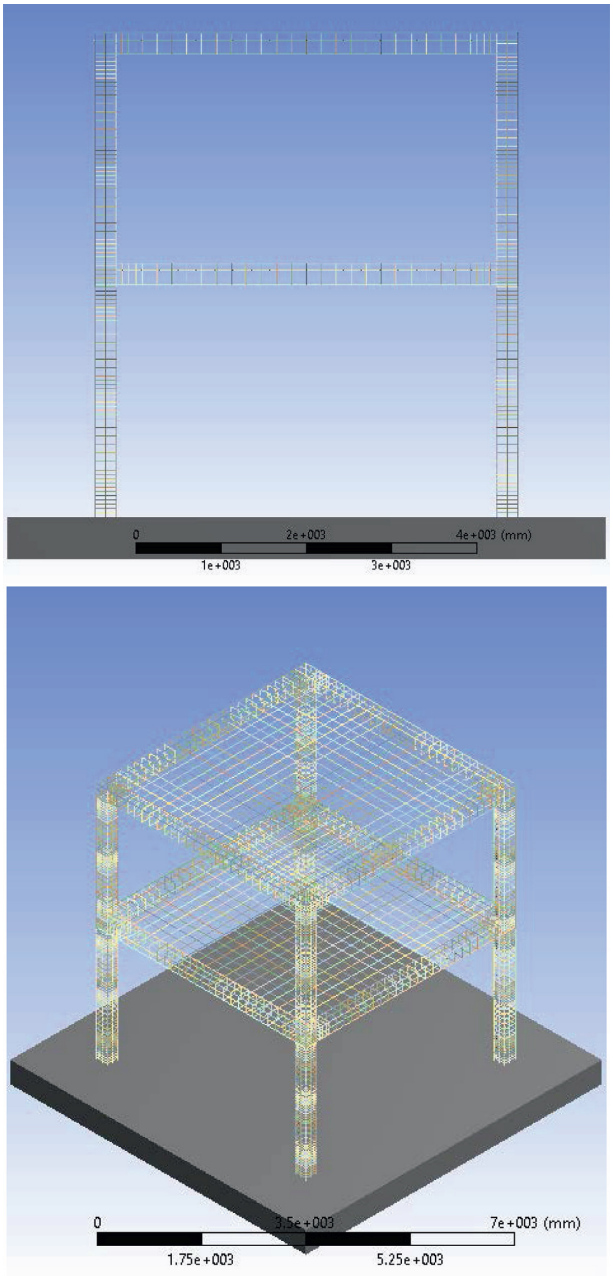

Figure 15: Reinforcement detailing for FRM_REI_DET_#3 on AUTODYN.

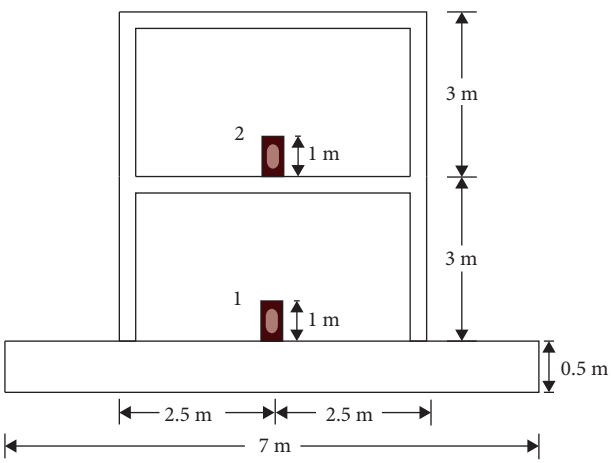

Figure 16: Locations of TNT explosives.

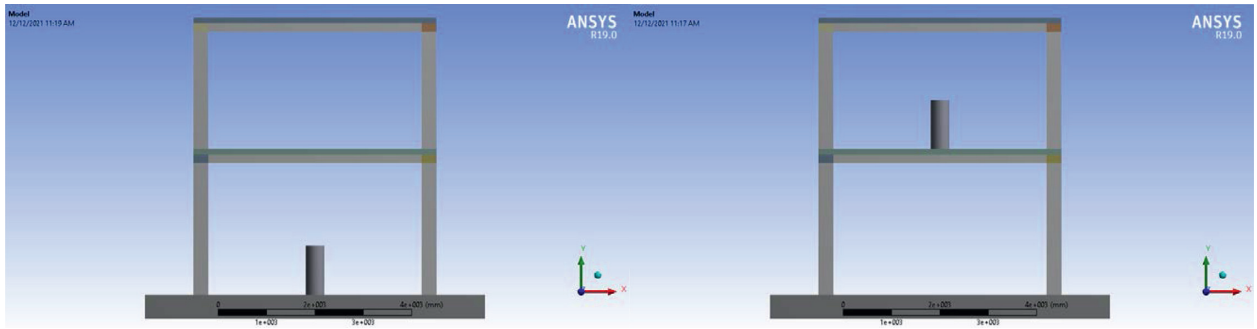

(a)

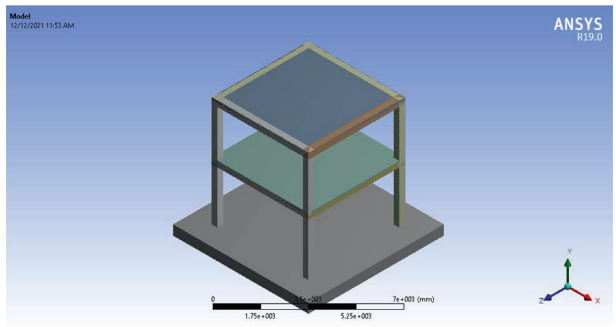

(b)

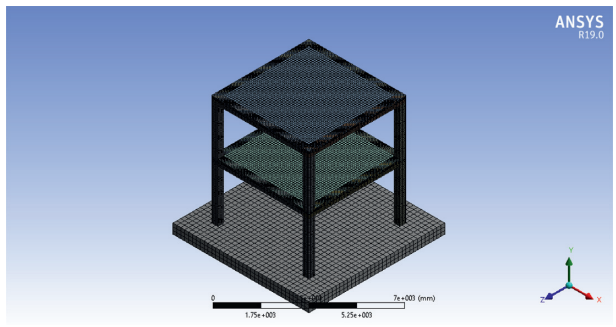

(c)

Figure 17: ANUTODYN FEA model with (a) location of TNT explosive, (b) 3D plot, and (c) meshes.

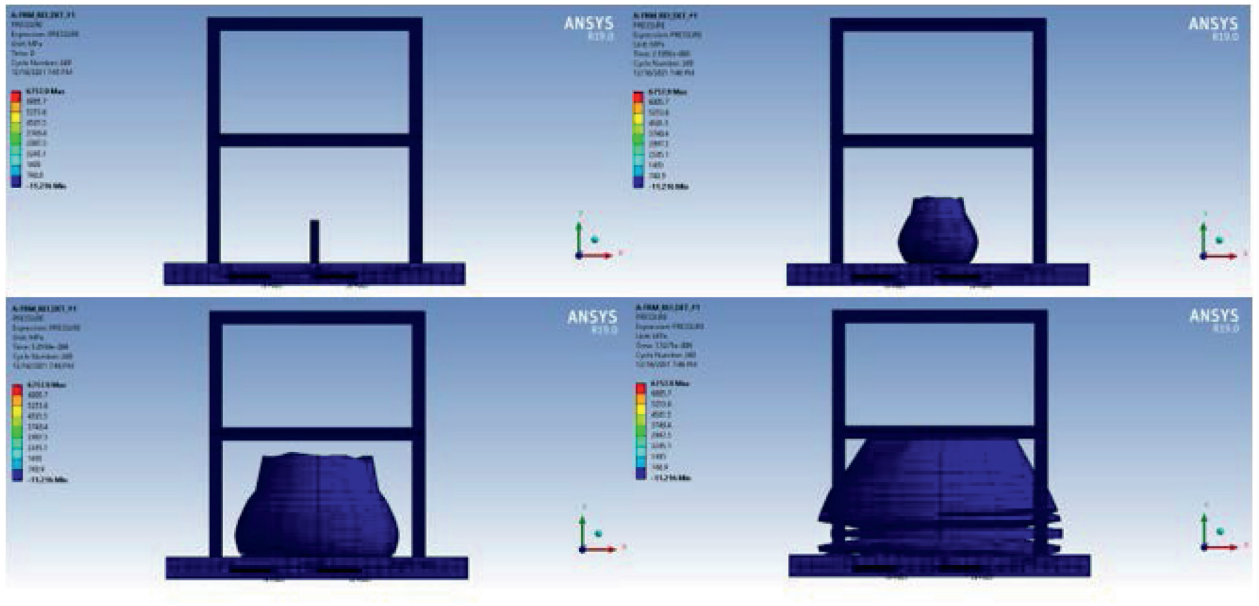

(a)

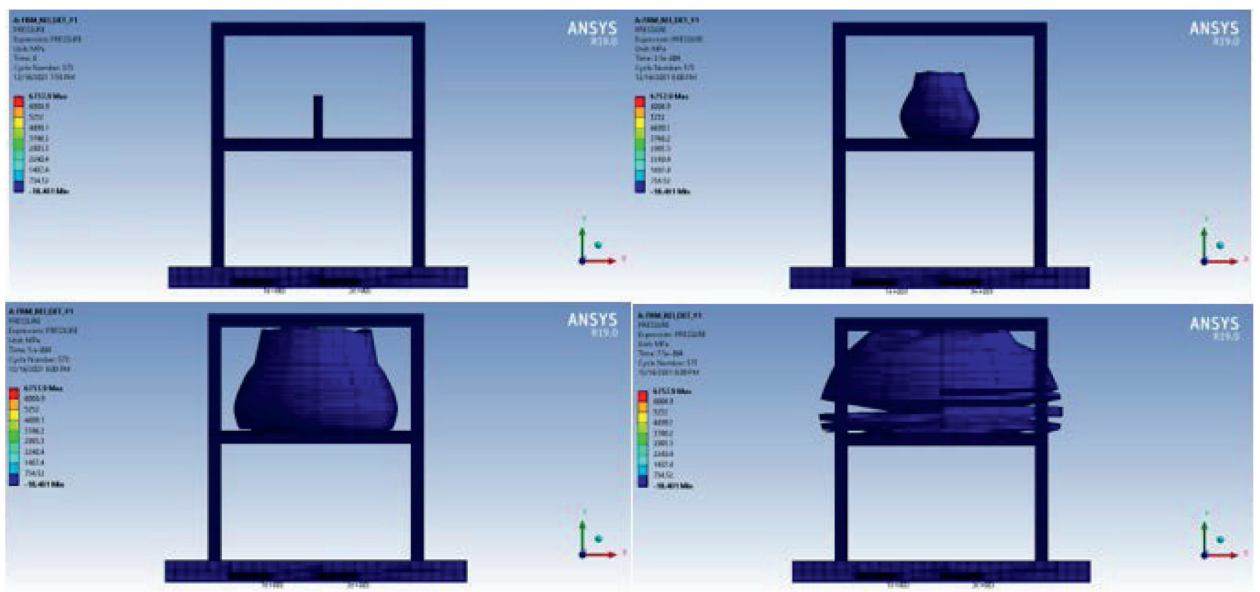

(b)

Figure 18: Blast pressure wave propagation time for two blast scenarios.

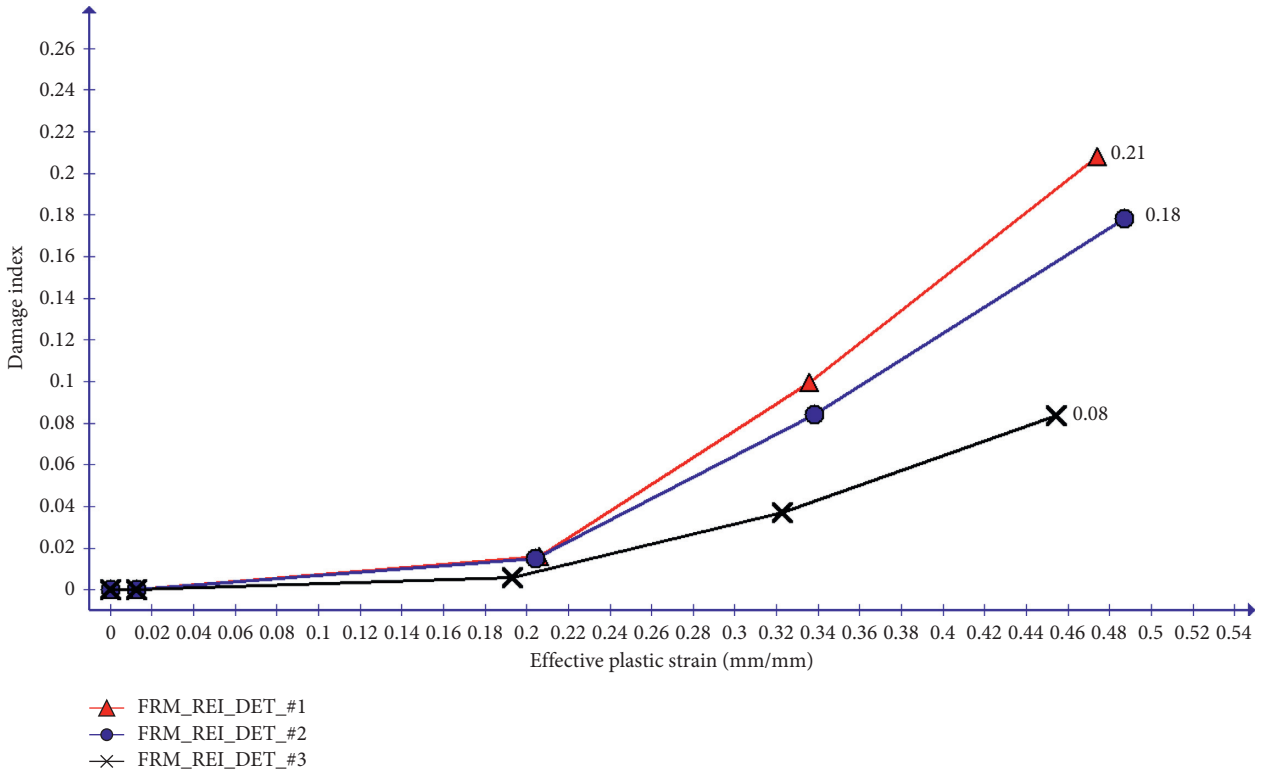

Figure 19: Column damage index vs. effective plastic strain plot for 46 kg TNT explosive located at 1st story ground floor slab.

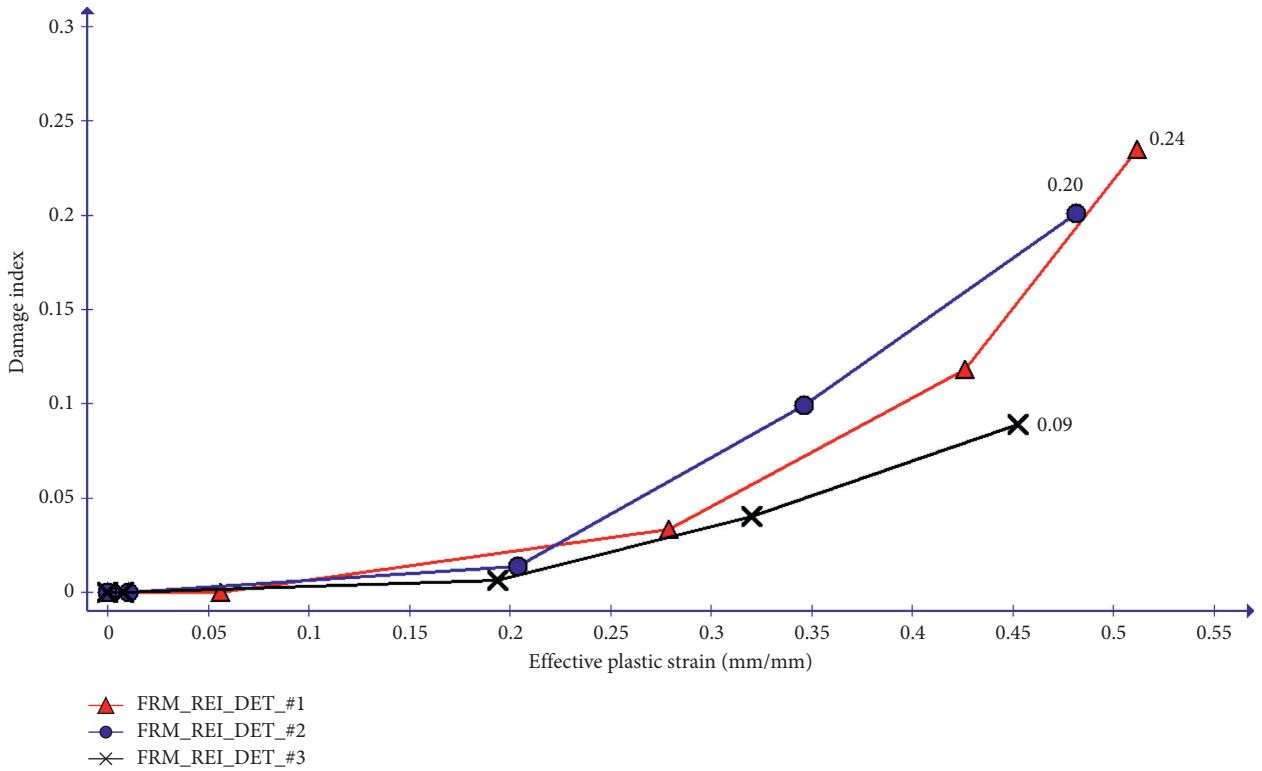

Figure 20: Column damage index vs. effective plastic strain plot for 46 kg TNT explosive located at 2nd story floor slab.

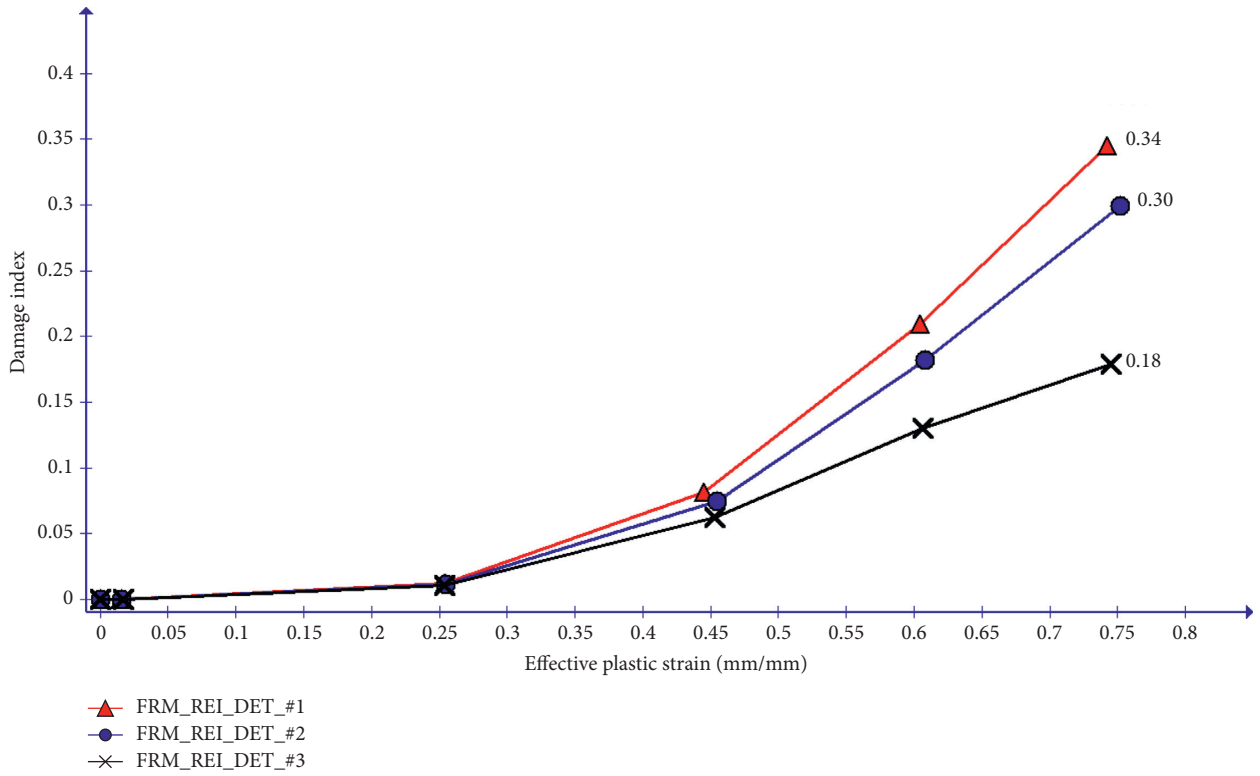

Figure 21: Column damage index vs. effective plastic strain plot for 91 kg TNT explosive located at 1st story ground floor slab.

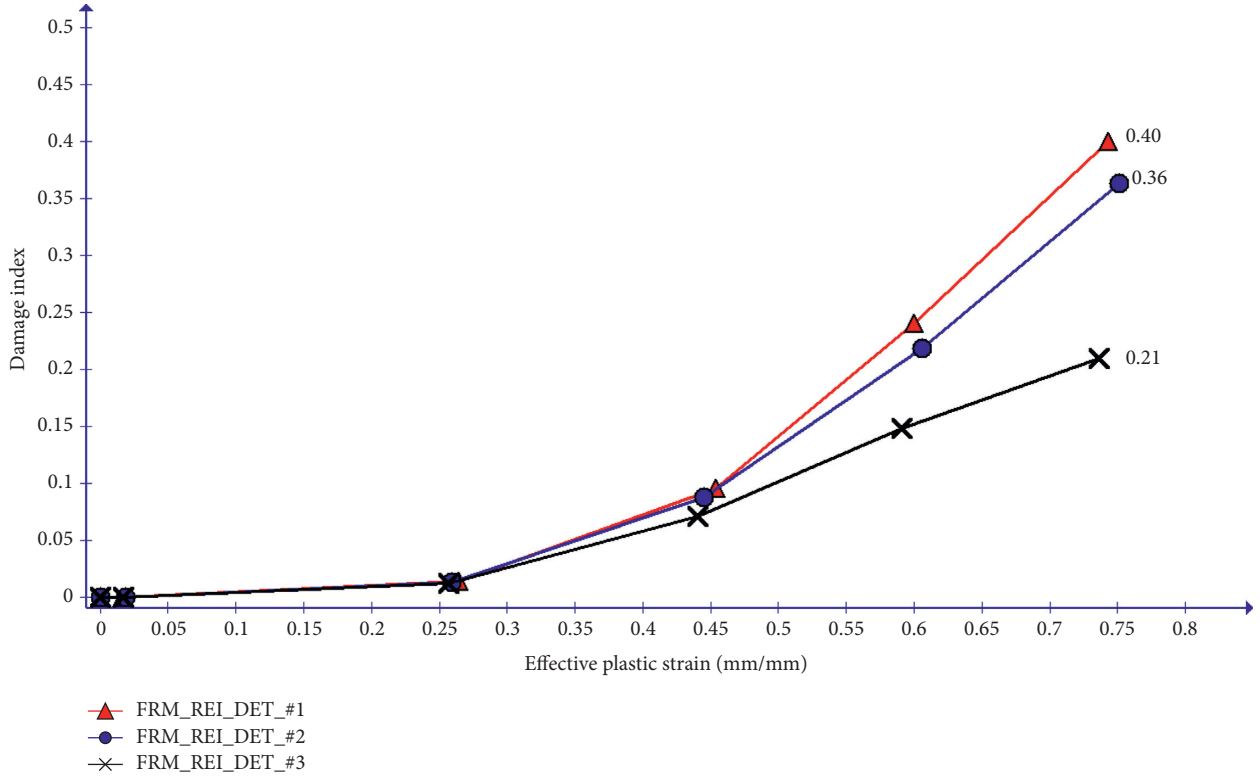

Figure 22: Column damage index vs. effective plastic strain plot 91 kg TNT explosive located at the 2nd story floor slab.

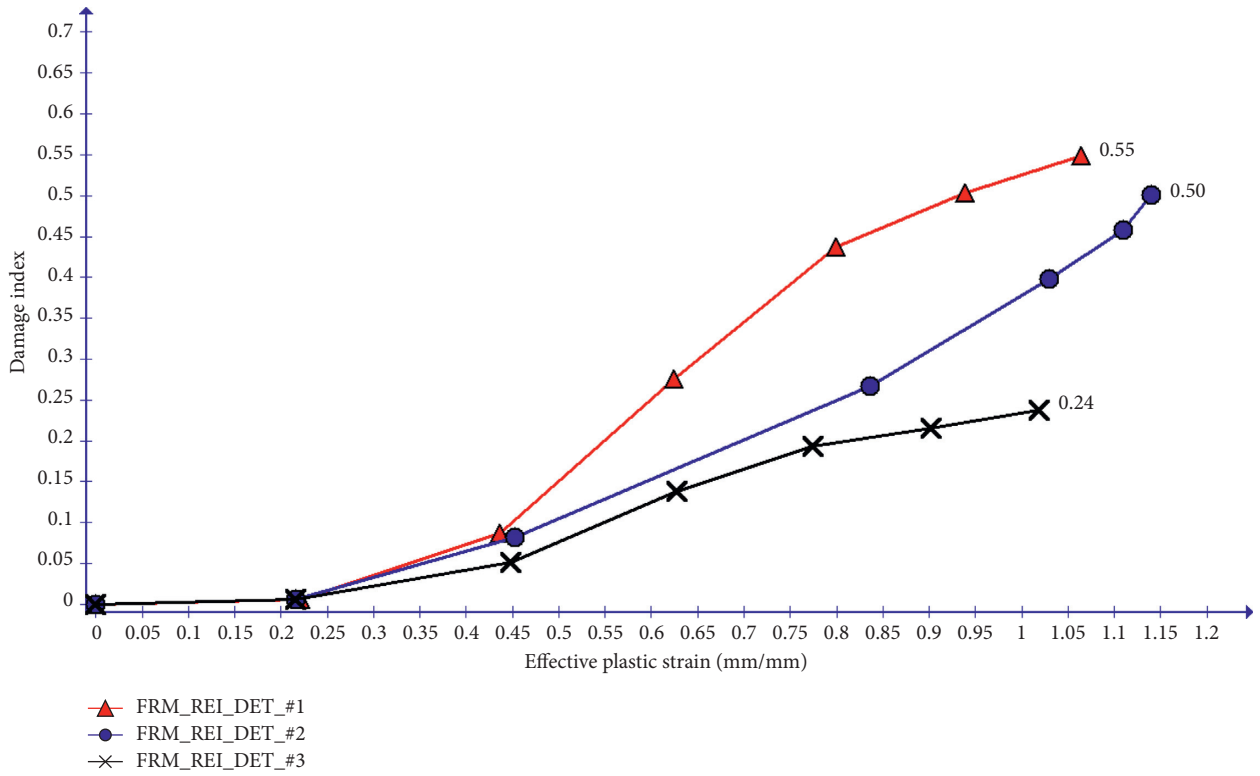

Figure 23: Column damage index vs. effective plastic strain plot for 215 kg TNT explosive located at 1st story ground floor slab.

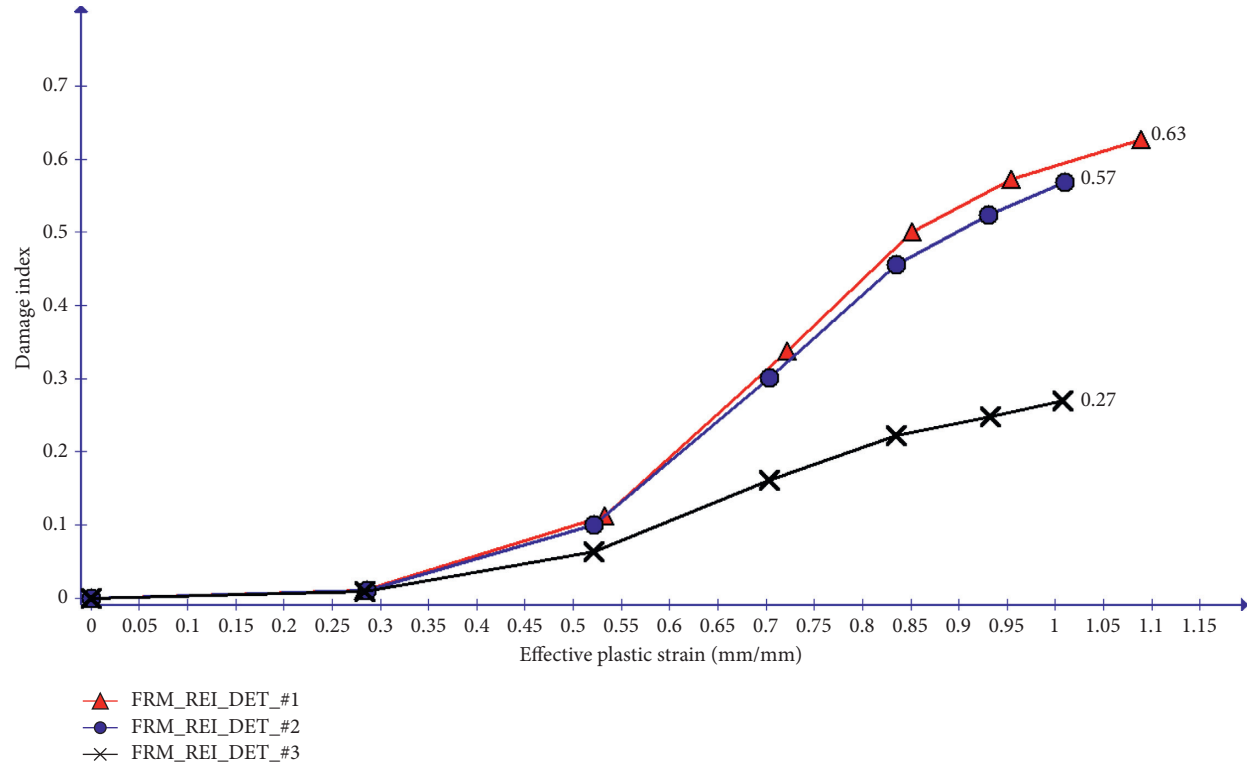

Figure 24: Column damage index vs. effective plastic strain plot for 215 kg TNT explosive located at 2nd story floor slab.

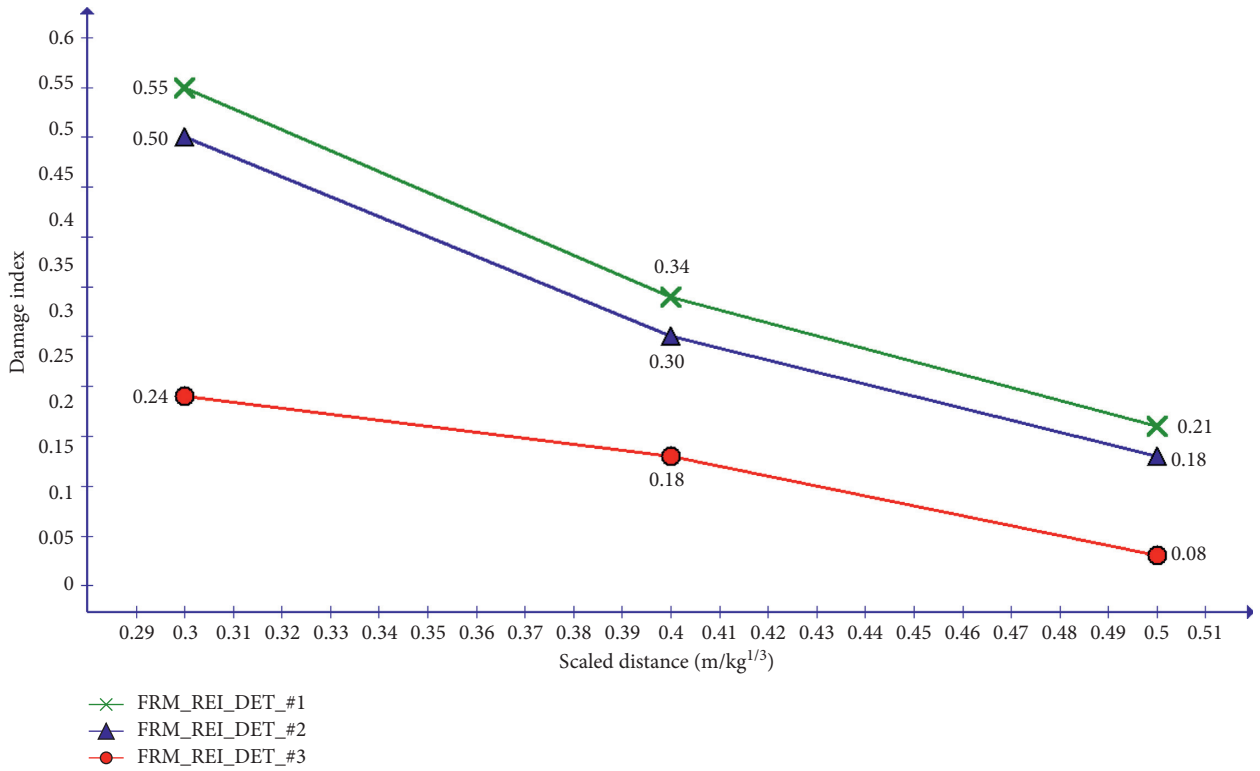

Figure 25: 1st story column damage index values for different reinforcement detailing provisions under various scaled distances.

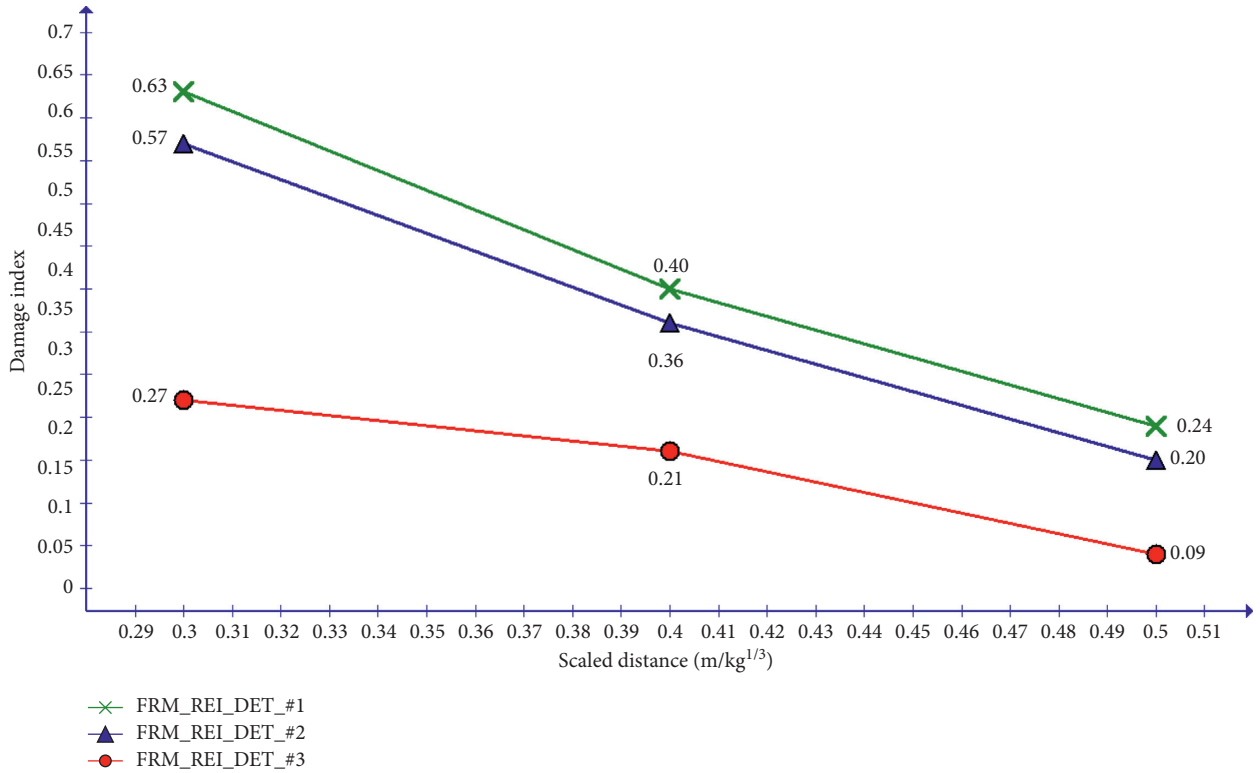

Figure 26: 2nd story column damage index values for different reinforcement detailing provisions under various scaled distances.

6. Conclusion

The present research investigated the structural performance assessment of two-story, one-bay conventional, and seismic resistant reinforced concrete framed buildings under close-in blast loading. Influential variables such as charge mass, explosive scaled distances, and various reinforcement detail provisions are studied to get insight into the blast load resistance of a reinforced concrete frame structure. Next, the major findings of the study are summarized.

(i) For a given close-in blast event, the decrease in scaled distance parameter increased, which results in effective plastic strain and damage indices

(ii) Minimizing transverse steel reinforcement spacing in a column significantly caused a drop in damage indices

(iii) Comparing seismic deficient columns with seismically detailed RC columns and having various blast scenarios with different scaled distances, the simultaneous use of closed spaced transverse steel reinforcement spacings in ends and midheight of reinforced concrete columns is found to be highly effective in reducing both effective plastic strains and damage index values

Data Availability

All data are included in the manuscript.

Conflicts of Interest

The authors declare that they have no conflicts of interest.

References

[1] G. Valsamos, M. Larcher, and F. Casadei, "Beirut explosion 2020: a case study for a large-scale urban blast Simulation," *Journal of Safety Science*, vol. 137, 2021.

[2] J. Jayasooriya, *Vulnerability and Damage Analysis of Reinforced Concrete Framed Buildings Subjected to Near-Field Blast Events*, Queensland University of Technology, Australia, 2010.

[3] S.-E. Kim and D.-K. Thai, "Numerical investigation of the damage of RC members subjceted to blast loading," *Engineering Failure Analysis*, vol. 92, pp. 350–367, 2018.

[4] Y. Temsah, J. Ali, J. Khatib, and M. Sonebi, "Numerical analysis of a reinforced concrete beam under blast loading," *MATEC Web of Conferences*, vol. 149, pp. 1–5, 2018.

[5] Li Chen, B. Rao, F. Qin, J. Hong, Z.-xian Liu, and H. b. Xiang, "Dynamic response of reinforced concrete beams under double-end-initiated close-in explosion," *Defence Technology*, vol. 14, pp. 527–539, 2018.

[6] S. Andersson and H. Karlsson, *Structural Response of Reinforced concrete Beams Subjected to Explosions*, Göteborg, Sweden, 2012.

[7] D. Rajkumar, R. Senthil, B. M. Kumar, and K. A. Gomathi, "Numerical study on parametric analysis of reinforced concrete column under blast loading," *Journal of Performance of Constructed Facilities*, vol. 1, p. 12, 2020.

[8] S. Astarlioglu, T. Krauthammer, D. Morency, and T. P. Tran, "Behavior of reinforced concrete columns under combined effects of axial and blast-induced transverse loads," *Engineering Structures*, vol. 55, pp. 26–34, 2013.

[9] B. Li, A. Nair, and K. Qian, "Residual axial capacity of reinforced concrete columns with simulated blast loading," *Journal of Performance of Constructed Facilities*, vol. 287, p. 299, 2012.

[10] Z. Wenjiao, X. Kong, Y. Qu, and Q. Zhao, "Numerical simulation of cracked reinforced concrete slabs subjected to blast loading," *Civil Engineering Journal*, vol. 4, no. 2, pp. 320–333, 2018.

[11] N. K. Vijitha, A. B. Pau, and R. Ahani, "Prediction of blast loading and its effects on waffle slab," *International Journal for Research in Applied Science and Engineering Technology*, vol. 5, pp. 864–871, 2017.

[12] J. K. R. Nalagotla, *Pressure-impulse Diagrams Using Finite Element Analysis for Reinforced concrete Slabs Subjected to Blast Loading*, University of Missouri-Kansas, Kansas, MO, USA, 2013.

[13] P. Vinothini and S. Elavenil, "Analytical investigation of high rise building under blast loading," *Indian Journal of Science and Technology*, vol. 9, no. 18, pp. 1–9, 2016.

[14] H. Draganić and V. Sigmund, "Blast loading on structures," *Tehnički Vjesnik*, vol. 19, pp. 643–652, 2012.

[15] Q. Kashif and M. B. Varma, "Effect of blast on G+4 RCC frame structure," *International Journal of Emerging Technology and Advanced Engineering*, vol. 4, no. 11, Article ID 145149, 2014.

[16] P. Tewari and A. Sharma, "Effects of blast loading on building frames," *International Research Journal of Engineering and Technology (IRJET)*, vol. 05, no. 5, pp. 4063–4069, 2018.

[17] R. G. Williams, W. A. Wilson, and R. Dookeeram, "Analysis of the response of a one-storey one-bay steel frame to blast," *Journal of Structures*, vol. 2016, Article ID 8571542, 11 pages, 2016.

[18] M. Murali and V. Sujisha, "Study on the response of RC frames subjected to blast loading," *International Journal of Engineering Research and Technology*, vol. 5, no. 08, pp. 602–607, 2016.

[19] A. T. Toy and B. Sevim, "Structural response of two-storey reinforced concrete building under blasting effects," *CBU J. of Sci*, vol. 12, no. 3, pp. 419–426, 2016.

[20] F. Siba, *Near-Field Explosion Effects on Reinforced Concrete Columns: An Experimental Investigation*, Carleton University, Ottawa, Canada, 2014.

[21] *ANSYS AUTODYN R19.0*, ANSYS, Inc., Canonsburg, PA, USA.

[22] R. M. Brannon and S. Leelavanichkul, *Survey of Four Damage Models for Concrete*, Sandia National Laboratories, California, 2009.

[23] W. Riedel and T. Borrvall, "The RHT concrete model in LS-DYNA," in *Proceedings of the 8th European LS-DYNA User Conference*, pp. 1–14, Strasbourg, France, January 2011.

[24] T. Borrvall, "The RHT concrete model in LS-DYNA," *8th European LS-DYNA User Conference*, vol. 1–15, 2011.

[25] C. Heckotter and J. Sievers, "Comparison of the RHT concrete material model in LS-DYNA and ansys autodyn," in *Proceedings of the 11th European LS-DYNA Conference*, pp. 1–16, Salzburg, Austria, 2017.

[26] J. Ekstrom, *Concrete Structures Subjected to Blast Loading*, Goteborg, 2015.

[27] E. Lee, M. Finger, and W. Collins, *JWL Equation of State Coefficients for High Explosives*, Lawrence Livermore Laboratory, California, 1973.

[28] H. Hamashima, Y. Kato, N. You, and S. Iloh, "Determination of JWL parameters from underwater explosion test for ideal and non-ideal explosives," *Science and Technology of Energetic Materials*, vol. 64, no. 6, pp. 248–253, 2003.

[29] L. E. Schwer, "Jones-wilken-lee (JWL) equation of state with afterburing," in *Proceedings of the 14th International LS-DYNA User Conference*, vol. 1–38, Windsor, CA, USA, July 2016.

[30] S. B. Segletes, *An Examination of the JWL Equation of State*, United States of America: US Army Research Laboratory, Aberdeen, Scotland, 2018.

[31] EN, *Eurocode 2: Design of Concrete Structures - Part 1: General Rules and Rules for Buildings pr EN1992*, Brussels, Belgium, 2002.

[32] EN, *Eurocode 8: Design of Structures for Earthquake Resistance, Part 1: General Rules, Seismic Actions, and Rules for Buildings EN1998-1-1*, Brussels, Belgium, 2003.